
Multi-Objective Nanobody Design via Masked Discrete Diffusion with Simplex Refinement

Rosie Ruoxi Zhang¹ Pranam Chatterjee^{2,3,†}

¹Penn Institute for Computational Science, University of Pennsylvania

²Department of Computer and Information Science, University of Pennsylvania

³Department of Bioengineering, University of Pennsylvania

[†]Correspondence to: pranam@seas.upenn.edu

Abstract

Nanobodies are compact, stable, and highly specific binding proteins that can access epitopes inaccessible to conventional antibodies, making them ideal scaffolds for therapeutic design. We present a masked discrete denoising framework for nanobody generation (*NanoMDLM*) that learns to reconstruct CDRs on a fixed scaffold, with region-specific masking that emphasizes diversity in CDR3. For inference, we develop a platform for Nanobody Optimization for Selective Interaction and Enhanced properties (**NOSIE**) via discrete simplex refinement (*DSR*), a gradient-free, black-box guidance method that samples CDR completions and reweights them using Pareto-weighted softmax over predicted binding and stability scores. At inference time, *DSR* steers *NanoMDLM* toward high-performing sequences without retraining or differentiable reward access. Across multiple antigens, including the GPCR MRGPRX2, **NOSIE** produces nanobodies with competitive or superior *in silico* binding, thermostability, and CDR3 quality, as assessed by NanoNet structure prediction, AlphaFold-Multimer co-folding, and feature combination-based ranking. Together, these results provide a scalable, sequence-only framework for multi-objective nanobody design, enabling numerous therapeutic applications.

1 Introduction

Nanobodies, or VHH single-domain antibodies derived from camelids, are compact, stable, and highly specific binding proteins with the ability to access recessed epitopes [Jovčevska and Muyldermans, 2020, Jin et al., 2023, Salvador et al., 2019, Uchański et al., 2020]. Their binding is localized to three complementarity-determining regions (CDRs), with CDR3 contributing most to antigen specificity [Mitchell and Colwell, 2018]. While *in silico* design offers a scalable alternative to screening [Longsompurana et al., 2023, Ferraz et al., 2025], optimizing nanobody CDRs for binding, stability, and developability remains challenging [Tadokoro et al., 2024]. Structure-based methods such as RFantibody, a fine-tuned variant of RFDiffusion, enable scaffold-aware CDR design [Watson et al., 2023, Sumida et al., 2024, Bennett et al., 2025] but require reliable co-complex structures. In contrast, masked denoising language models (MDLMs) offer a scalable, sequence-only alternative and have been applied across protein design tasks [Sahoo et al., 2024, Shi et al., 2024, Wang et al., 2024, Goel et al., 2025, Tang et al., 2025, Vincoff et al., 2025a]. Prior guidance strategies, including CFG [Ho and Salimans, 2022], LaMBO-2/NOS [Gruver et al., 2023], and PepTune [Tang et al., 2025], focus on full-sequence optimization but are not tailored to modular settings like nanobody CDR design. Here, we introduce **NanoMDLM**, a CDR-constrained MDLM trained with region-dependent masking, and combine it with a new inference-time framework, **discrete simplex refinement (DSR)**, for Nanobody Optimization for Selective Interaction and Enhanced properties (**NOSIE**). *DSR* guides

generation using black-box predictors for binding and thermostability via Pareto-weighted sampling, without requiring gradients or retraining (Figure 1). Across multiple antigens, including the GPCR MRGPRX2, our framework produces nanobody candidates that outperform or match structure-based methods in binding, stability, and CDR3 plausibility.

Our contributions:

- A nanobody-specific masked denoising model (NanoMDLM) with CDR-only corruption and region-weighted masking.
- A gradient-free guidance method (DSR) that optimizes multi-objective reward via reweighted sampling over the categorical simplex.
- A unified framework (NOSIE) that achieves strong *in silico* nanobody design performance without relying on structural input.

2 Problem Formulation

We present NOSIE, a framework for guided nanobody generation via masked discrete denoising and inference-time optimization. See Appendix Sections C and D for full data and architectural details.

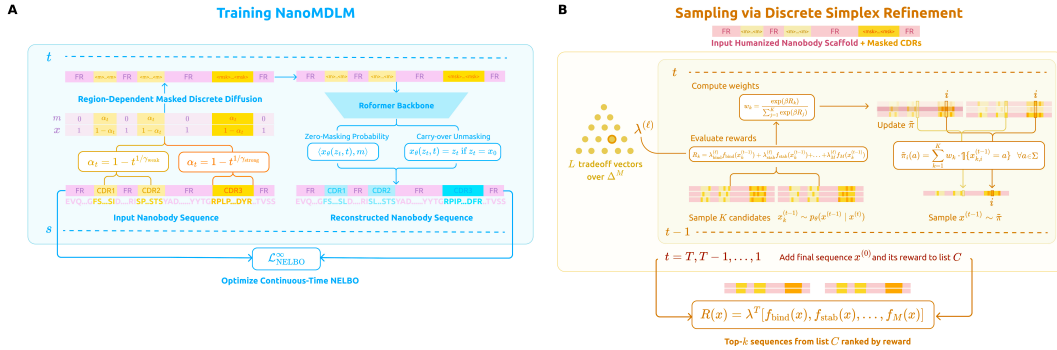


Figure 1: **Overview of NOSIE.** A: Continuous-time training of discrete masked diffusion model NanoMDLM under Region-Specific masking schedules, with SUBS parametrization and RoFormer as the denoising backbone. B: Sampling with Discrete Simplex Refinement (DSR) where humanized scaffolds with masked CDRs are iteratively refined by candidate sampling, reward evaluation, and tradeoff vector weighting, producing ranked sequences with optimized multi-objective performance.

2.1 CDR-Constrained Masked Denoising

Let $x \in \Sigma^L$ denote a nanobody sequence, partitioned into framework (FR) and complementarity-determining regions (CDRs):

$$x = (x_{FR1}, x_{CDR1}, x_{FR2}, x_{CDR2}, x_{FR3}, x_{CDR3}, x_{FR4}),$$

with mutable positions $\mathcal{C} = \{CDR1, CDR2, CDR3\}$. Framework residues are fixed during training and generation.

The forward corruption process over T timesteps applies region-specific masking strengths $\gamma(i)$:

$$\gamma(i) = \begin{cases} \gamma_{\text{weak}} & \text{if } i \in \text{CDR1 or CDR2,} \\ \gamma_{\text{strong}} & \text{if } i \in \text{CDR3,} \end{cases} \quad \text{with } \gamma_{\text{strong}} > \gamma_{\text{weak}}.$$

Given a global schedule $\alpha_t \in [0, 1]$, corruption proceeds as:

$$q(x^{(t)} | x^{(t-1)}) = \prod_{i \in \mathcal{C}} \text{Cat}(x_i^{(t)} | \alpha_t^{\gamma(i)} \delta_{x_i^{(t-1)}} + (1 - \alpha_t^{\gamma(i)})u),$$

where u is the uniform amino acid distribution. The denoising model learns to invert this process by minimizing:

$$\mathcal{L}_{\text{MDLM}} = \mathbb{E}_{t, x^{(0)}, x^{(t)} \sim q} \left[- \sum_{i \in \mathcal{C}} \log p_{\theta}(x_i^{(0)} | x^{(t)}) \right].$$

2.2 Discrete Simplex Refinement (DSR)

At inference, we guide generation using black-box reward models $f_{\text{bind}}, f_{\text{stab}} : \Sigma^L \rightarrow \mathbb{R}$ for binding and thermostability. At each step t , we sample K completions $\{x_k^{(t-1)}\}_{k=1}^K$ and compute scalarized rewards:

$$R_k^{(\lambda)} = \lambda_{\text{bind}} f_{\text{bind}}(x_k^{(t-1)}) + \lambda_{\text{stab}} f_{\text{stab}}(x_k^{(t-1)}),$$

with weights $\lambda \in \Delta^2$. The candidates are softmax-reweighted:

$$w_k = \frac{\exp(\beta R_k^{(\lambda)})}{\sum_j \exp(\beta R_j^{(\lambda)})},$$

and the categorical logits are updated via:

$$\tilde{\pi}_i^{(t)}(a) = \sum_{k=1}^K w_k \cdot \mathbb{1}\{x_{k,i}^{(t-1)} = a\}, \quad \forall i \in \mathcal{C}.$$

2.3 Optimization Objective

This update is equivalent to solving the following KL-regularized mirror descent step:

$$\tilde{\pi}^{(t)} = \arg \min_{\pi \in \Delta^{|\Sigma|^{|C|}}} \text{KL}(\pi || \pi^{(t)}) - \eta \sum_{k=1}^K R_k^{(\lambda)} \log \pi(x_k),$$

which guarantees ascent in expected scalarized reward at each step (see Appendix B).

3 Results

3.1 Guided Generation Scores

We evaluated NOSIE across a panel of antigens by comparing it to unconditional sampling and MCTS-guided optimization from PepTune [Tang et al., 2025], using DeepNano [Deng et al., 2024] and NanoMelt [Ramon et al., 2025] to assess predicted binding and thermostability. For PD-L1 (Figure 2), both guidance methods outperform the unconditional baseline, with NOSIE consistently producing top-ranked candidates with stronger antigen interaction and improved stability. This pattern holds across additional antigens (Figure A7), where NOSIE frequently matches or exceeds experimental binders in affinity while maintaining favorable developability. In harder cases such as CTLA-4 (7DV4_1, Figure A7-F) [Gan et al., 2022], where reference binders are near-optimal, NOSIE still produces stable and competitive alternatives, suggesting that simplex-guided denoising is effective even in narrow design spaces.

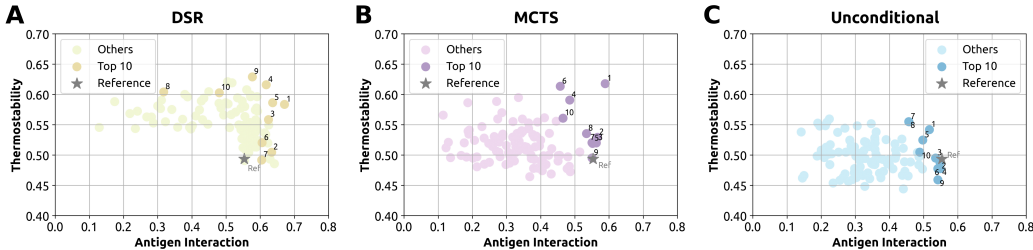


Figure 2: **Comparison of generated nanobody scores with antigen PD-L1.** Reference point represents the scores of the known binding VHH (PDB: 7CZD_2). All three sampling methods were run with 32 sampling timesteps. For unconditional and MCTS methods, the top 100 sequences were ranked by the average of the antigen interaction and thermostability scores, whereas NOSIE sequences were ranked according to scalar rewards defined by the algorithm.

3.2 Validation on MRGPRX2

MRGPRX2 is an orphan GPCR involved in IgE-independent hypersensitivity, making it a biologically relevant target for nanobody design [Al Hamwi et al., 2025]. We selected it due to its shallow pocket and because AF-Multimer shows strong discriminative performance on this antigen [Al Hamwi et al., 2022, Evans et al., 2021, Harvey et al., 2025]. We compared 20 NOSIE-generated nanobodies to 20 RFantibody sequences [Bennett et al., 2025], using AFM-based metrics including LCF [Harvey et al., 2025], ipTM, pAE, and pDockQ. Despite using only antigen sequence, NOSIE matched or outperformed RFantibody across all metrics (Table 1), achieving higher ipTM, lower pAE, and equivalent LCF with less variance. Predicted complexes show confident binding interfaces and plausible CDR3 structures (Figure 3), highlighting NOSIE’s ability to generate high-quality nanobodies without structural input.

Table 1: Comparison of average AFM metrics (mean with SEM in parentheses) across 20 pilot nanobody sequences targeting MRGPRX2, generated with RFantibody (RFa) and NOSIE, evaluated using the best-ranked AFM model for each complex. The input to RFa-AF is an AF2 predicted structure of MRGPRX2, while the input to RFa-PDB is the PDB:7VV6 structure of MRGPRX2.

Method	LCF \uparrow	pTM \uparrow	ipTM \uparrow	pAE \downarrow	pDockQ \uparrow
RFa-AF	0.039 (0.006)	0.679 (0.011)	0.402 (0.031)	15.637 (0.830)	0.290 (0.025)
RFa-PDB	0.045 (0.009)	0.690 (0.013)	0.428 (0.051)	14.401 (1.335)	0.317 (0.042)
NOSIE	0.045 (0.005)	0.681 (0.011)	0.450 (0.031)	13.289 (0.637)	0.288 (0.018)

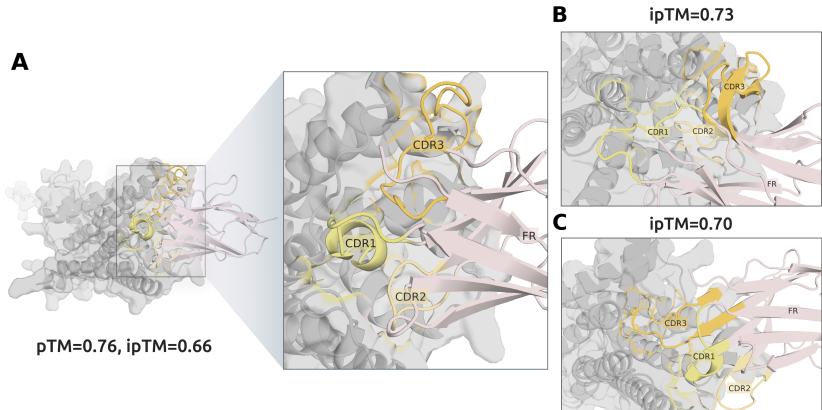


Figure 3: AlphaFold2-Multimer-predicted structures of the three top NOSIE nanobody binders to MRGPRX2

4 Discussion

Our results show that CDR-constrained masked discrete denoising, combined with black-box simplex refinement, enables nanobody design without structural input or differentiable objectives. By masking only the CDRs (especially CDR3) and guiding generation via Pareto-weighted reweighting, NOSIE efficiently produces high-quality sequences. Compared to RFantibody Bennett et al. [2025], our method achieves competitive or superior performance in predicted binding, buried surface area, and thermostability. NOSIE is readily extensible to other reward functions (i.e., immunogenicity, pH sensitivity, expression) and is being integrated with high-throughput experimental screening Xia et al. [2025]. Looking ahead, conditioning on isoform-specific Vincoff et al. [2025b,a] or PTM-specific Peng et al. [2025] signals may enable precision targeting of disease-relevant proteoforms, supporting a new class of programmable nanobody therapeutics.

References

- Ivana Jovčevska and Serge Muyldermans. The therapeutic potential of nanobodies. *BioDrugs*, 34(1): 11–26, 2020.
- Bo-Kyung Jin, Steven Odongo, Magdalena Radwanska, and Stefan Magez. Nanobodies@: a review of diagnostic and therapeutic applications. *International journal of molecular sciences*, 24(6): 5994–5994, 2023.
- J-Pablo Salvador, Lluïsa Vilaplana, and M-Pilar Marco. Nanobody: outstanding features for diagnostic and therapeutic applications. *Analytical and bioanalytical chemistry*, 411(9):1703–1713, 2019.
- Tomasz Uchański, Els Pardon, and Jan Steyaert. Nanobodies to study protein conformational states. *Current opinion in structural biology*, 60:117–123, 2020.
- Laura S Mitchell and Lucy J Colwell. Comparative analysis of nanobody sequence and structure data. *Proteins: Structure, Function, and Bioinformatics*, 86(7):697–706, 2018.
- Phoomintara Longsompurana, Thanyada Rungrotmongkol, Nongluk Plongthongkum, Kittikhun Wangkanont, Peter Wolschann, and Rungtiva P Poo-Arporn. Computational design of novel nanobodies targeting the receptor binding domain of variants of concern of sars-cov-2. *Plos one*, 18(10):e0293263, 2023.
- Matheus VF Ferraz, W Camilla S Adan, Tayná E Lima, Adriele JC Santos, Sérgio O de Paula, Rafael Dhalia, Gabriel L Wallau, Rebecca C Wade, Isabelle FT Viana, and Roberto D Lins. Design of nanobody targeting sars-cov-2 spike glycoprotein using cdr-grafting assisted by molecular simulation and machine learning. *PLOS Computational Biology*, 21(4):e1012921, 2025.
- Takashi Tadokoro, Harumi Tsuboi, Kota Nakamura, Tetsushi Hayakawa, Reo Ohmura, Izumi Kato, Masaki Inoue, Shin-ichi Tsunoda, Sayaka Niizuma, Yukari Okada, et al. Thermostability and binding properties of single-chained fv fragments derived from therapeutic antibodies. *Protein Science*, 33(7):e5084, 2024.
- Joseph L Watson, David Juergens, Nathaniel R Bennett, Brian L Trippe, Jason Yim, Helen E Eisenach, Woody Ahern, Andrew J Borst, Robert J Ragotte, Lukas F Milles, et al. De novo design of protein structure and function with rfdiffusion. *Nature*, 620(7976):1089–1100, 2023.
- Kiera H Sumida, Reyes Núñez-Franco, Indrek Kalvet, Samuel J Pellock, Basile IM Wicky, Lukas F Milles, Justas Dauparas, Jue Wang, Yakov Kipnis, Noel Jameson, et al. Improving protein expression, stability, and function with proteinmpnn. *Journal of the American Chemical Society*, 146(3):2054–2061, 2024.
- Nathaniel R Bennett, Joseph L Watson, Robert J Ragotte, Andrew J Borst, DéJenaé L See, Connor Weidle, Riti Biswas, Yutong Yu, Ellen L Shrock, Russell Ault, et al. Atomically accurate de novo design of antibodies with rfdiffusion. *bioRxiv*, pages 2024–03, 2025.
- Subham Sahoo, Marianne Arriola, Yair Schiff, Aaron Gokaslan, Edgar Marroquin, Justin Chiu, Alexander Rush, and Volodymyr Kuleshov. Simple and effective masked diffusion language models. *Advances in Neural Information Processing Systems*, 37:130136–130184, 2024.
- Jiaxin Shi, Kehang Han, Zhe Wang, Arnaud Doucet, and Michalis Titsias. Simplified and generalized masked diffusion for discrete data. In *The Thirty-eighth Annual Conference on Neural Information Processing Systems*, 2024. URL <https://openreview.net/forum?id=xcqS0fHt4g>.
- Xinyou Wang, Zaixiang Zheng, Fei YE, Dongyu Xue, Shujian Huang, and Quanquan Gu. Diffusion language models are versatile protein learners. In *Forty-first International Conference on Machine Learning*, 2024. URL <https://openreview.net/forum?id=NUAbSFqyqb>.
- Shrey Goel, Vishrut Thoutam, Edgar Mariano Marroquin, Aaron Gokaslan, Arash Firouzbakht, Sophia Vincoff, Volodymyr Kuleshov, Huong T Kratochvil, and Pranam Chatterjee. Memdlm: De novo membrane protein design with property-guided discrete diffusion. In *Learning Meaningful Representations of Life (LMRL) Workshop at ICLR 2025*, 2025.

- Sophia Tang, Yinuo Zhang, and Pranam Chatterjee. Peptune: De novo generation of therapeutic peptides with multi-objective-guided discrete diffusion. In *Forty-second International Conference on Machine Learning*, 2025. URL <https://openreview.net/forum?id=FQoy1Y1Hd8>.
- Sophia Vincoff, Oscar Davis, Ismail Ilkan Ceylan, Alexander Tong, Joey Bose, and Pranam Chatterjee. SOAPIA: Siamese-guided generation of off target-avoiding protein interactions with high target affinity. In *ICML 2025 Workshop on Scaling Up Intervention Models*, 2025a. URL <https://openreview.net/forum?id=j00pIG71eX>.
- Jonathan Ho and Tim Salimans. Classifier-free diffusion guidance. *arXiv preprint arXiv:2207.12598*, 2022.
- Nate Gruver, Samuel Stanton, Nathan Frey, Tim GJ Rudner, Isidro Hotzel, Julien Lafrance-Vanasse, Arvind Rajpal, Kyunghyun Cho, and Andrew G Wilson. Protein design with guided discrete diffusion. *Advances in neural information processing systems*, 36:12489–12517, 2023.
- Juntao Deng, Miao Gu, Pengyan Zhang, Mingyu Dong, Tao Liu, Yabin Zhang, and Min Liu. Nanobody–antigen interaction prediction with ensemble deep learning and prompt-based protein language models. *Nature Machine Intelligence*, 6(12):1594–1604, 2024.
- Aubin Ramon, Mingyang Ni, Olga Predeina, Rebecca Gaffey, Patrick Kunz, Shimobi Onuoha, and Pietro Sormanni. Prediction of protein biophysical traits from limited data: a case study on nanobody thermostability through nanomelt. *mAbs*, 17(1), January 2025. ISSN 1942-0870. doi: 10.1080/19420862.2024.2442750. URL <http://dx.doi.org/10.1080/19420862.2024.2442750>.
- Xin Gan, Qianqian Shan, He Li, Rick Janssens, Yuqiang Shen, Yun He, Fei Chen, Rien Van Haperen, Dubravka Drabek, Jin Li, et al. An anti-ctla-4 heavy chain–only antibody with enhanced treg depletion shows excellent preclinical efficacy and safety profile. *Proceedings of the National Academy of Sciences*, 119(32):e2200879119, 2022.
- Ghazl Al Hamwi, Mohamad Wessam Alnouri, Sven Verdonck, Piotr Leonczak, Shaswati Chaki, Stefan Frischbutter, Pavel Kolkhir, Michaela Matthey, Constantin Kopp, Marek Bednarski, et al. Subnanomolar mas-related g protein-coupled receptor-x2/b2 antagonists with efficacy in human mast cells and disease models. *Signal transduction and targeted therapy*, 10(1):128, 2025.
- Ghazl Al Hamwi, Yvonne K Riedel, Sophie Clemens, Vigneshwaran Namasivayam, Dominik Thimm, and Christa E Müller. Mas-related g protein-coupled receptors x (mrgprx): Orphan gpcrs with potential as targets for future drugs. *Pharmacology & Therapeutics*, 238:108259, 2022.
- Richard Evans, Michael O’Neill, Alexander Pritzel, Natasha Antropova, Andrew Senior, Tim Green, Augustin Židek, Russ Bates, Sam Blackwell, Jason Yim, et al. Protein complex prediction with alphafold-multimer. *bioRxiv*, pages 2021–10, 2021.
- Edward P Harvey, Jeffrey S Smith, Joseph D Hurley, Alyana Granados, Ernst W Schmid, Jason G Liang-Lin, Steffanie Paul, Emily M Meara, Matthew P Ferguson, Victor G Calvillo-Miranda, et al. In silico discovery of nanobody binders to a g-protein coupled receptor using alphafold-multimer. *bioRxiv*, pages 2025–03, 2025.
- Baolong Xia, Ah-Ram Kim, Feimei Liu, Myeonghoon Han, Emily Stoneburner, Stephanie Makdissi, Francesca Di Cara, Stephanie E Mohr, Aaron M Ring, and Norbert Perrimon. Phage-displayed synthetic library and screening platform for nanobody discovery. *eLife*, June 2025. doi: 10.7554/eLife.105887.2. URL <http://dx.doi.org/10.7554/eLife.105887.2>.
- Sophia Vincoff, Shrey Goel, Kseniia Kholina, Rishab Pulugurta, Pranay Vure, and Pranam Chatterjee. Fuson-plm: a fusion oncoprotein-specific language model via adjusted rate masking. *Nature Communications*, 16(1), February 2025b. ISSN 2041-1723. doi: 10.1038/s41467-025-56745-6. URL <http://dx.doi.org/10.1038/s41467-025-56745-6>.
- Fred Zhangzhi Peng, Chentong Wang, Tong Chen, Benjamin Schussheim, Sophia Vincoff, and Pranam Chatterjee. Ptm-mamba: a ptm-aware protein language model with bidirectional gated mamba blocks. *Nature Methods*, 22(5):945–949, April 2025. ISSN 1548-7105. doi: 10.1038/s41592-025-02656-9. URL <http://dx.doi.org/10.1038/s41592-025-02656-9>.

- Jian Ma, Fandi Wu, Tingyang Xu, Shaoyong Xu, Wei Liu, Divin Yan, Qifeng Bai, and Jianhua Yao. An adaptive autoregressive diffusion approach to design active humanized antibody and nanobody. *bioRxiv*, pages 2024–10, 2024.
- Constantin Schneider, Matthew IJ Raybould, and Charlotte M Deane. Sabdab in the age of biotherapeutics: updates including sabdab-nano, the nanobody structure tracker. *Nucleic acids research*, 50(D1):D1368–D1372, 2022.
- Cecile Vincke, Remy Loris, Dirk Saerens, Sergio Martinez-Rodriguez, Serge Muyldermans, and Katja Conrath. General strategy to humanize a camelid single-domain antibody and identification of a universal humanized nanobody scaffold. *Journal of Biological Chemistry*, 284(5):3273–3284, 2009.
- Jianlin Su, Murtadha Ahmed, Yu Lu, Shengfeng Pan, Wen Bo, and Yunfeng Liu. Roformer: Enhanced transformer with rotary position embedding. *Neurocomputing*, 568:127063, 2024.
- Matthew IJ Raybould, Claire Marks, Alan P Lewis, Jiye Shi, Alexander Bujotzek, Bruck Taddese, and Charlotte M Deane. Thera-sabdab: the therapeutic structural antibody database. *Nucleic acids research*, 48(D1):D383–D388, 2020.

A Algorithm

We present the full pseudocode for nanobody generation via masked discrete denoising and inference-time multi-objective guidance. The framework comprises two stages: training a CDR-constrained MDLM, and guided generation using discrete simplex refinement.

Algorithm 1 Training CDR-Constrained MDLM for Nanobody Generation

- 1: **Input:** Nanobody sequence dataset \mathcal{D} , scaffold mask \mathcal{S} , CDR mask \mathcal{C} , corruption schedule $\{\alpha_t\}_{t=1}^T$, CDR-specific exponents $\gamma_{\text{weak}}, \gamma_{\text{strong}}$
- 2: **for** each training step **do**
- 3: Sample sequence $x^{(0)} \sim \mathcal{D}$
- 4: Initialize $x^{(t)} \leftarrow x^{(0)}$
- 5: **for** each position $i \in \mathcal{C}$ **do**
- 6: Determine $\gamma(i) \leftarrow \begin{cases} \gamma_{\text{weak}}, & i \in \text{CDR1 or CDR2} \\ \gamma_{\text{strong}}, & i \in \text{CDR3} \end{cases}$
- 7: Sample masking with probability $1 - \alpha_t^{\gamma(i)}$
- 8: **end for**
- 9: Construct corrupted input $x^{(t)}$ with sampled masks; leave $x_j^{(t)} = x_j^{(0)}$ for $j \in \mathcal{S}$
- 10: Compute model logits $p_{\theta}(x_i^{(0)} | x^{(t)})$ for $i \in \mathcal{C}$
- 11: Compute cross-entropy loss:

$$\mathcal{L}_{\text{MDLM}} = - \sum_{i \in \mathcal{C}} \log p_{\theta}(x_i^{(0)} | x^{(t)})$$

- 12: Update model parameters θ using gradient $\nabla_{\theta} \mathcal{L}_{\text{MDLM}}$
 - 13: **end for**
-

Algorithm 2 Multi-Objective Discrete Simplex Refinement (DSR) for Nanobody Generation

1: **Input:** Trained MDLM $p_\theta(x^{(t-1)} | x^{(t)})$, reward models $f_{\text{bind}}, f_{\text{stab}}$, temperature β , number of tradeoffs L , number of seeds S , candidates per seed K , top- k output size
2: Generate tradeoff vectors $\{\lambda^{(\ell)}\}_{\ell=1}^L$ over Δ^2 (e.g., via Das-Dennis lattice)
3: Initialize empty list $\mathcal{C} \leftarrow \emptyset$
4: **for** $\ell = 1$ to L **do** ▷ Loop over tradeoff weights
5: **for** $s = 1$ to S **do** ▷ Loop over independent seeds
6: Initialize $x^{(T)} \sim \text{MASKED_CDR_NOISE}()$
7: **for** $t = T$ to 1 **do**
8: Sample $\{x_k^{(t-1)}\}_{k=1}^K \sim p_\theta(x^{(t-1)} | x^{(t)})$
9: **for** $k = 1$ to K **do**
10: Evaluate rewards:
$$R_k = \lambda_{\text{bind}}^{(\ell)} f_{\text{bind}}(x_k^{(t-1)}) + \lambda_{\text{stab}}^{(\ell)} f_{\text{stab}}(x_k^{(t-1)})$$

11: **end for**
12: Compute softmax weights:
$$w_k = \frac{\exp(\beta R_k)}{\sum_{j=1}^K \exp(\beta R_j)}$$

13: **for** each CDR position $i \in \mathcal{C}$ **do**
14: **for** each token $a \in \Sigma$ **do**
15: Update:
$$\tilde{\pi}_i(a) = \sum_{k=1}^K w_k \cdot \mathbb{1}\{x_{k,i}^{(t-1)} = a\}$$

16: **end for**
17: **end for**
18: Sample $x^{(t-1)}$ from $\tilde{\pi}$ at each $i \in \mathcal{C}$
19: **end for**
20: Add final sequence $x^{(0)}$ and its reward to list \mathcal{C}
21: **end for**
22: **end for**
23: Sort \mathcal{C} by scalarized reward: $R(x) = \lambda^T [f_{\text{bind}}(x), f_{\text{stab}}(x)]$
24: **Return:** Top- k nanobody sequences from \mathcal{C}

B Discrete Simplex Refinement Proof

We provide a proof that Discrete Simplex Refinement (DSR) updates at each denoising step guarantee a monotonic improvement in expected scalarized reward.

Theorem B.1 (DSR Monotonic Improvement). *Let $\pi^{(t)}$ be the uniform distribution over K samples $\{x_k\}_{k=1}^K$ drawn from the base model at timestep t , i.e., $\pi^{(t)}(x_k) = \frac{1}{K}$ for all k . Let $R_k := R^{(\lambda)}(x_k) \in \mathbb{R}$ be the corresponding scalarized rewards. Define the DSR-updated distribution as:*

$$\tilde{\pi}^{(t)}(x_k) := \frac{\exp(\beta R_k)}{\sum_{j=1}^K \exp(\beta R_j)} =: w_k,$$

where $\beta > 0$ is the temperature parameter. Then:

$$\mathbb{E}_{x \sim \tilde{\pi}^{(t)}}[R(x)] \geq \mathbb{E}_{x \sim \pi^{(t)}}[R(x)],$$

with strict inequality whenever the rewards $\{R_k\}$ are not all equal.

Proof. The expected reward under the original uniform distribution is:

$$\mathbb{E}_{x \sim \pi^{(t)}}[R(x)] = \sum_{k=1}^K \frac{1}{K} R_k = \frac{1}{K} \sum_{k=1}^K R_k.$$

The expected reward under the DSR-updated distribution is:

$$\mathbb{E}_{x \sim \tilde{\pi}^{(t)}}[R(x)] = \sum_{k=1}^K w_k R_k = \sum_{k=1}^K \frac{\exp(\beta R_k)}{\sum_{j=1}^K \exp(\beta R_j)} R_k.$$

To establish monotonic improvement, we show that:

$$\sum_{k=1}^K w_k R_k \geq \frac{1}{K} \sum_{k=1}^K R_k.$$

Case 1: If all rewards are equal, i.e., $R_k = c$ for some constant c and all k , then:

$$w_k = \frac{\exp(\beta c)}{\sum_{j=1}^K \exp(\beta c)} = \frac{\exp(\beta c)}{K \exp(\beta c)} = \frac{1}{K},$$

so $\tilde{\pi}^{(t)} = \pi^{(t)}$ and equality holds.

Case 2: If the rewards are not all equal, we use the following key lemma:

Lemma B.2 (Softmax Improvement Property). *For any non-constant vector (R_1, \dots, R_K) and $\beta > 0$:*

$$\sum_{k=1}^K \frac{\exp(\beta R_k)}{\sum_{j=1}^K \exp(\beta R_j)} R_k > \frac{1}{K} \sum_{k=1}^K R_k.$$

Proof of Lemma. Define $f(\beta) = \sum_{k=1}^K \frac{\exp(\beta R_k)}{\sum_{j=1}^K \exp(\beta R_j)} R_k$. Note that:

- $f(0) = \frac{1}{K} \sum_{k=1}^K R_k$ (uniform weighting)
- $f'(\beta) = \text{Var}_{\text{softmax}_\beta}(R) \geq 0$, with strict inequality when R_k are not all equal

To see this, compute:

$$f'(\beta) = \sum_{k=1}^K w_k R_k^2 - \left(\sum_{k=1}^K w_k R_k \right)^2 = \mathbb{E}[R^2] - (\mathbb{E}[R])^2 = \text{Var}(R),$$

where the expectation is taken with respect to the softmax distribution with temperature β^{-1} .

Since $\text{Var}(R) > 0$ when R_k are not all equal, we have $f'(\beta) > 0$ for all $\beta > 0$. Therefore, $f(\beta) > f(0)$ for any $\beta > 0$. \square

C Data Curation and Processing

C.1 Pre-training Dataset and Tokenization

The pre-training dataset comprises 3,395,594 unpaired heavy chain sequences curated by HuDiff [Ma et al., 2024], sourced from the OAS database, and aligned using the IMGT numbering scheme. All sequences were aligned to a length of 152 residues. For tokenization, we employed an amino acid tokenizer with a vocabulary of 23 tokens, comprising the 20 canonical amino acids, an ‘X’ token for unknown residues, a ‘-’ token for padding, and a ‘<mask>’ token for masked positions.

C.2 Benchmark Dataset

The experimental antigens and their paired reference nanobodies were obtained from SAbDab-nano [Schneider et al., 2022]. After filtering for *Homo Sapiens* species, a resolution cutoff of 3.0 Å, and complexes containing only two molecules, the initial pool consisted of 35 complex structures. Manual screening was then performed to remove redundant antigens with identical sequences, yielding 25 distinct antigen sequences used for unconditional sequence generation screening in Figure A1.

C.3 Humanized Scaffold for Sampling Inference

During inference, we employed a universal humanized nanobody scaffold [Vincke et al., 2009] for the framework regions, while sampling the CDRs from our model. To construct the input sequence, the h-NbBcIII10_{FGLA} sequence was first aligned to a fixed length of 152 residues using the IMGT numbering scheme, consistent with our training sequences. The CDR regions were then substituted with mask tokens for model inference.

D NanoMDLM Implementation Details

D.1 Region-Dependent Masking

Building on state-dependent [Shi et al., 2024] and bond-dependent masking for peptides [Tang et al., 2025], we propose a masking schedule where the probability of masking tokens in CDR1 and CDR2 increases more slowly at early timesteps t compared to CDR3 tokens. This design reflects the more conserved nature of CDR1 and CDR2, while allowing greater diversity in CDR3 sequences (as shown in Figure A2). We define the discrete-time log-linear masking schedule $\sigma(t) = -\log(1 - t^{1/\gamma_{\text{weak}}})$ for CDR1 and CDR2, and the log-polynomial schedule $\sigma(t) = -\log(1 - t^{1/\gamma_{\text{strong}}})$ for CDR3.

The masking probabilities $\alpha_t = \exp(-\sigma(t))$ for the CDR tokens are thus:

$$\alpha_t^{\gamma(i)} = \begin{cases} 1 - t^{1/\gamma_{\text{weak}}} & \text{if } i \in \text{CDR1 or CDR2,} \\ 1 - t^{1/\gamma_{\text{strong}}} & \text{if } i \in \text{CDR3,} \end{cases} \quad \text{with } \gamma_{\text{strong}} > \gamma_{\text{weak}}.$$

In our implementation, we set $\gamma_{\text{weak}} = 1/3$ and $\gamma_{\text{strong}} = 1$.

For the forward corruption process $q(x^{(t)}|x^{(t-1)})$, this approach ensures a slower masking rate in CDR1 and CDR2 at earlier stages of the diffusion process, while CDR3 are masked more quickly with a stronger exponent γ_{strong} . This enables the model to first focus

D.2 Training Strategy and Model Architecture

Pretraining of NanoMDLM for nanobodies was conducted on 4 NVIDIA DGX B200 GPUs, using the AdamW optimizer with a learning rate of 0.0003 and weight decay of 0.075. At each reverse step, token probabilities are modeled using a RoFormer network [Su et al., 2024]. The full set of model hyperparameters is listed below.

Table 2: Roformer Architecture Hyperparameters

Hyperparameter	PepTune
Input Dimension	23 (vocab size)
Hidden Dimension	768
Intermediate Dimension	3072
Number of Layers	8
Attention Heads	8
Max Positional Embeddings	256
Hidden and Attention Dropout Probability	0.1

Table 3: Training and Validation Loss of NanoMDLM. Loss values are taken after convergence at 45 epochs when training NanoMDLM on 3 million unpaired human heavy chain sequences.

Model	Train Loss (\downarrow)	Train PPL (\downarrow)	Val Loss (\downarrow)	Val PPL (\downarrow)
Standard Masking	0.661	2.025	0.676	1.988
Region-Dependent Masking	0.600	1.983	0.642	1.948

E Scoring Models

Nanobody-Antigen Interaction. DeepNano [Deng et al., 2024] is a deep learning ensemble framework with a prompt-based mechanism that guides attention to antigen-binding sites, achieving state-of-the-art performance in nanobody-antigen interaction (NAI) prediction for virtual screening. We use its predicted interaction score as

$$f_{\text{bind}}(x) = \text{DeepNano}(x, y).$$

where y stands for the antigen sequence.

Thermostability. The thermostability score is based on NanoMelt [Ramon et al., 2025], a semi-supervised ensemble model for predicting the apparent melting temperatures of nanobodies. Since the model outputs raw melting temperatures, we regularize them to a $[0, 1]$ score using the linear transformation

$$f_{\text{stab}}(x) = \frac{\text{NanoMelt}(x) - T_{\min}}{T_{\max} - T_{\min}},$$

where T_{\min} and T_{\max} are taken from the distribution of the 640 training sequences.

F Additional Studies on Sampling

F.1 Unconditional Generation Quality

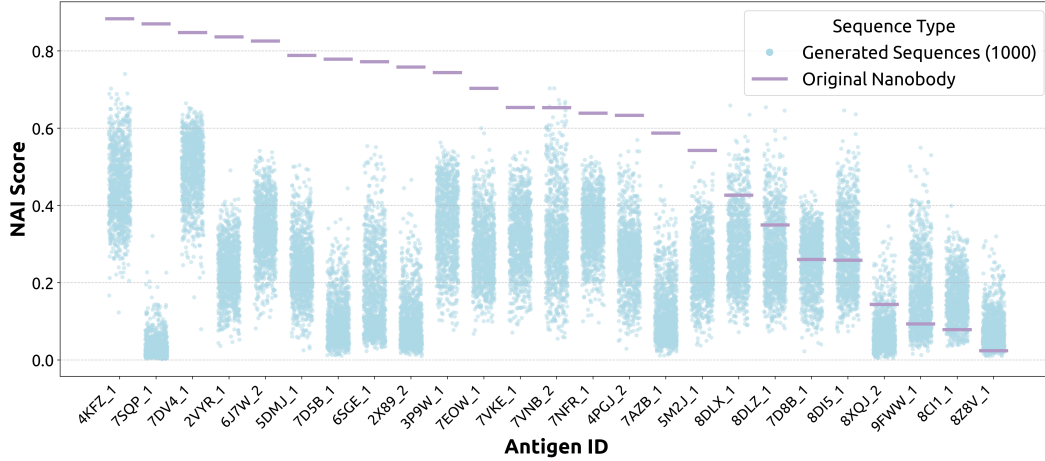


Figure A1: Interaction scores with human antigens of experimental and unconditionally generated nanobody sequences. Experimental human antigens and nanobody sequences were obtained from SAbDab-nano. After filtering for one-to-one interaction complexes and applying redundancy reduction, 25 distinct antigens were selected. Interaction scores were predicted using DeepNano. For each antigen, the score corresponding to its original experimental nanobody is shown as a purple line. Scores for 1,000 unconditionally generated nanobody sequences from the base MDLM are represented as skyblue dots.

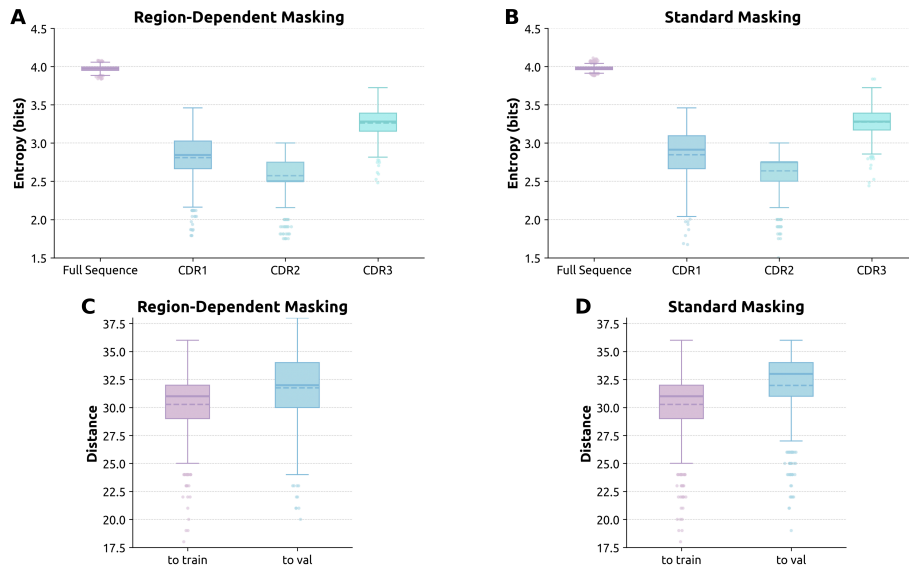


Figure A2: Unconditional-generated nanobody sequence analysis. A-B: Shannon entropy of the unconditionally generated sequences (N=1000); C-D: Minimum Levenshtein distance of the unconditionally generated sequences (N=1000)

To evaluate sequence diversity, we calculated Shannon entropy and Jaccard similarity. Shannon entropy $H(X) = -\sum p(x) \log_2 p(x)$ measures the variability of the amino acid distribution, with higher values indicating greater diversity. As shown in Figure A2 (Panels A-B), region-dependent masking results in slightly higher entropy across all CDR regions, suggesting it promotes greater sequence diversity, particularly in CDR3.

Jaccard similarity $J(A, B) = \frac{|A \cap B|}{|A \cup B|}$ assesses the overlap with reference sequences, with higher values indicating better fidelity. Table 4 shows that standard masking yields higher Jaccard similarity to the training and validation sequences, suggesting a stronger resemblance to the existing database. In contrast, region-specific masking slightly reduces similarity but increases diversity.

Table 4: Mean pairwise Jaccard similarity for unconditionally generated nanobody sequence (N=1000)

Masking Method	Full Sequence	CDR1	CDR2	CDR3
Standard Masking	0.980503	0.529960	0.511030	0.580592
Region-Specific Masking	0.977800	0.463944	0.418981	0.528402

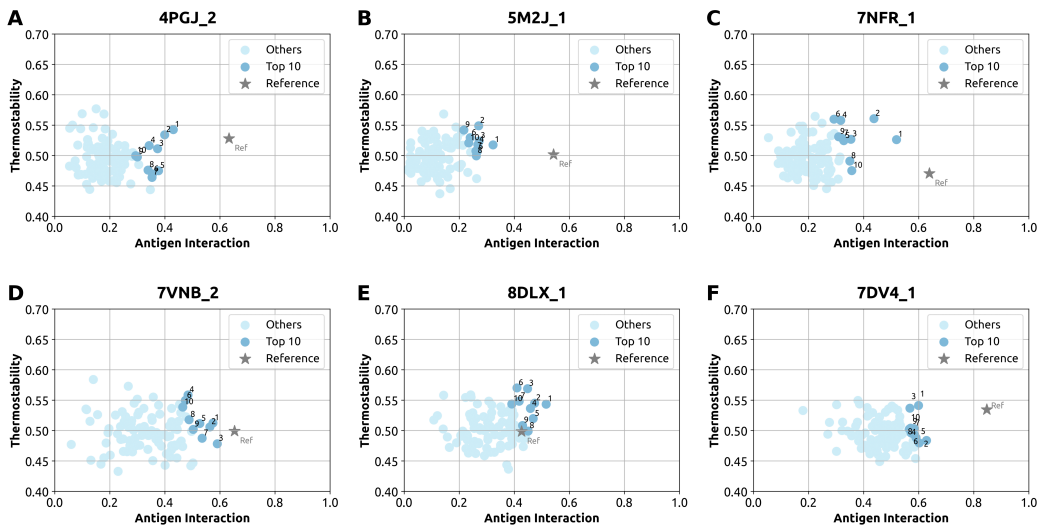


Figure A3: Scores of unconditionally generated nanobodies with selected antigens. The antigens in A-E are with experimental nanobodies that exhibit moderate interaction scores (0.4-0.65).

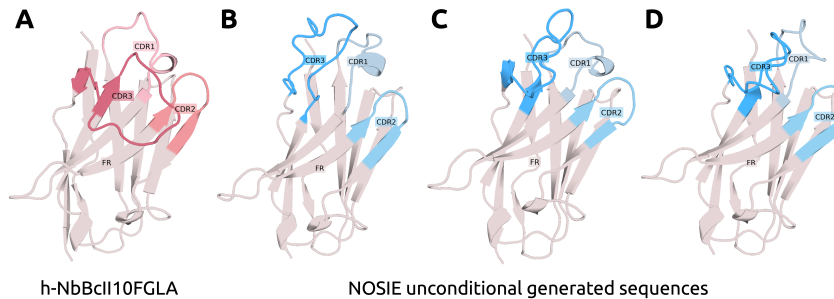


Figure A4: NanoNet-predicted structures of NbBCII10 humanized (FGLA mutant) and three NanoMDLM unconditional generated nanobodies

F.2 DSR Generation Quality

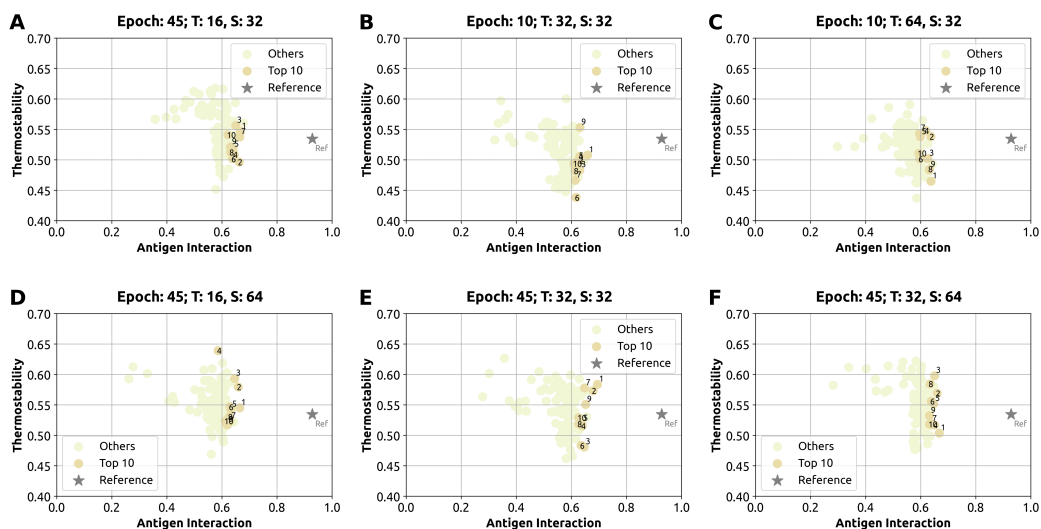


Figure A5: Hyperparameter search for DSR sampling conducted on antigen CTLA-4 (PDB:7DV4_1), topK=100.

Hyperparameter Search for DSR. In this analysis, we conducted a hyperparameter search for DSR sampling on antigen CTLA-4 [Gan et al., 2022]. In A5, each subplot compares different combinations of training epochs, sampling timesteps (T), and sampling seeds (S), showing the antigen interaction and thermostability scores of the top 100 sequences generated in each configuration. Panels B–C correspond to the base model trained for only 10 epochs. As observed, while the antigen interaction scores exhibit moderate variation, these shorter training runs result in noticeably lower thermostability scores. This suggests that longer training allows the base model to better capture the underlying biological properties of the CDRs. In contrast, the results from the epoch-45 base model (panels A, D–F) highlight that intermediate sampling timesteps and number of seeds—particularly in panels A, D–F—achieve a favorable balance, producing high-quality candidates while avoiding excessive variance.

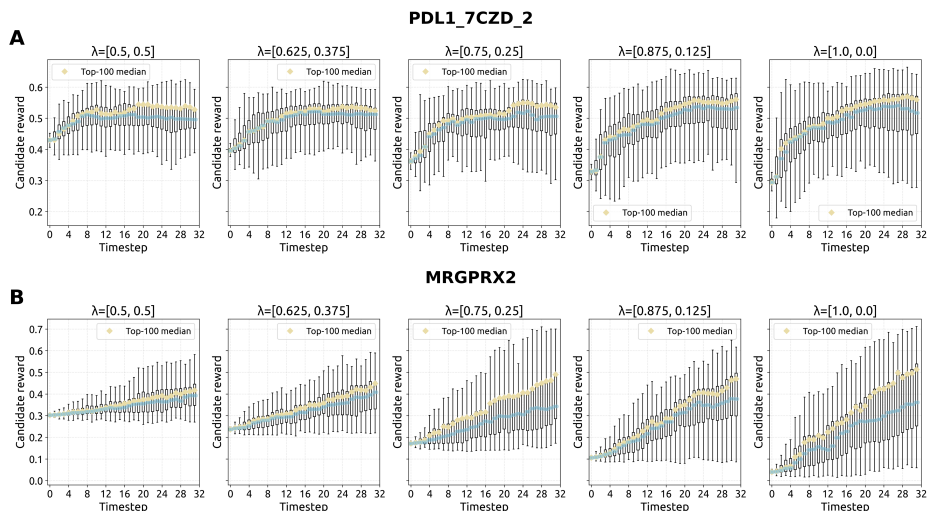


Figure A6: Candidate reward trajectories for NOSIE optimization on (A) PDL-1 and (B) MRGPRX2. Each panel corresponds to a different weighting scheme for the binding affinity term (λ). Boxplots show the distribution of candidate rewards at each timestep, while the yellow diamonds track the median reward of the final top-100 candidate sequences across timesteps.

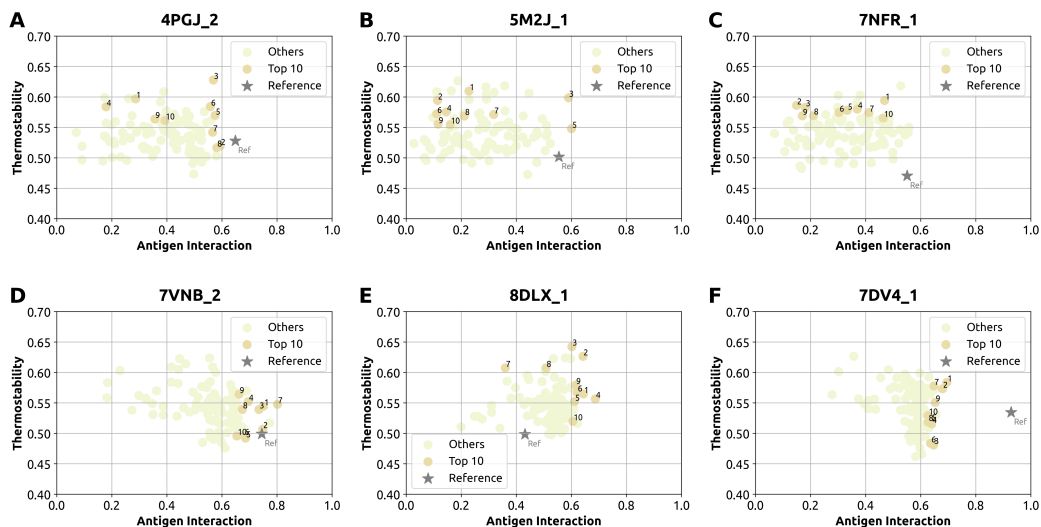


Figure A7: Scores of DSR-generated nanobodies with antigens from SAbDab-nano. The antigens in A-E are with experimental nanobodies that exhibit moderate interaction scores (0.4-0.65).

Validation on Therapeutic Antigens. To emphasize therapeutic applications that prioritize strong target engagement, we assign a weight of ≥ 0.5 to the nanobody–antigen interaction score for therapeutic antigens A8. Accordingly, we present NOSIE results for three clinically relevant targets—PD-L1, the SARS-CoV-2 Spike protein, and TNF—each of which has established clinical-stage nanobody candidates [Raybould et al., 2020]. Across these antigens, NOSIE generates sequences that not only achieve high binding affinity but also maintain favorable thermostability, underscoring the framework’s ability to balance multiple objectives relevant for therapeutic development. Importantly, NOSIE also generalizes to antigens without existing clinical-stage nanobodies, as demonstrated by

its performance on MRGPRX2, thereby highlighting its potential for broad applicability in both well-studied and novel therapeutic contexts.

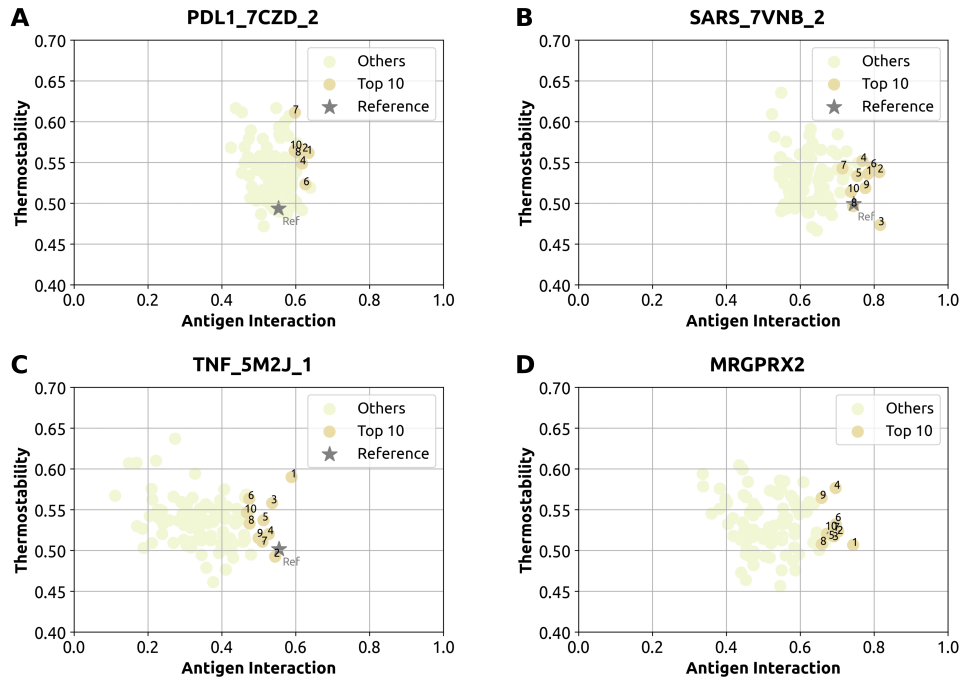


Figure A8: NOSIE-generated nanobody scores across therapeutic targets (A-C) PD-L1, SARS-Cov-2 Spike protein, TNF with clinical-stage nanobodies, and (D) MRGPRX2.

E.3 MCTS Generation Quality

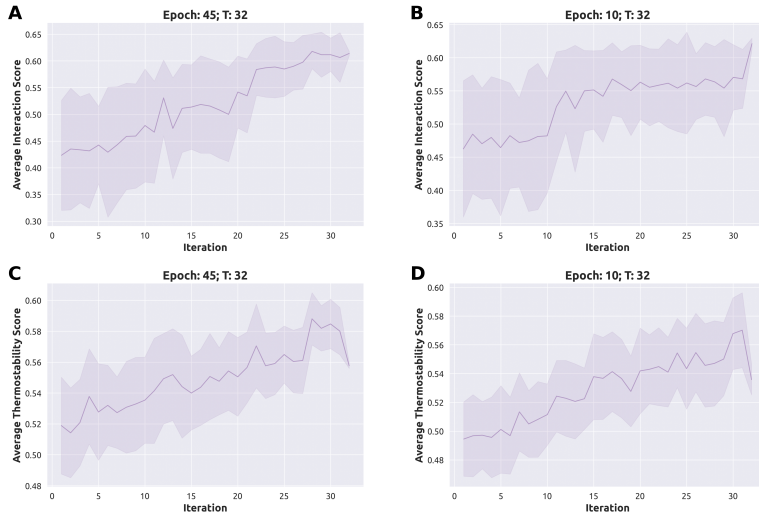


Figure A9: MCTS property scores over iteration on two epochs version of the base MDLM model

Figure A9 presents the progression of antigen interaction and thermostability scores among MCTS iterations for the two base MDLM models trained for 45 or 10 epochs. Consistent with previous observations in DSR sampling, panels B and D (10-epoch models) show that while antigen interaction scores improve with iterations, the thermostability scores remain comparatively lower than those of the 45-epoch models (panels A and C). This echoes the earlier finding that sufficient training until convergence enables the model to better capture the underlying biological properties of CDRs, leading to more stable and higher-quality sequence generation.

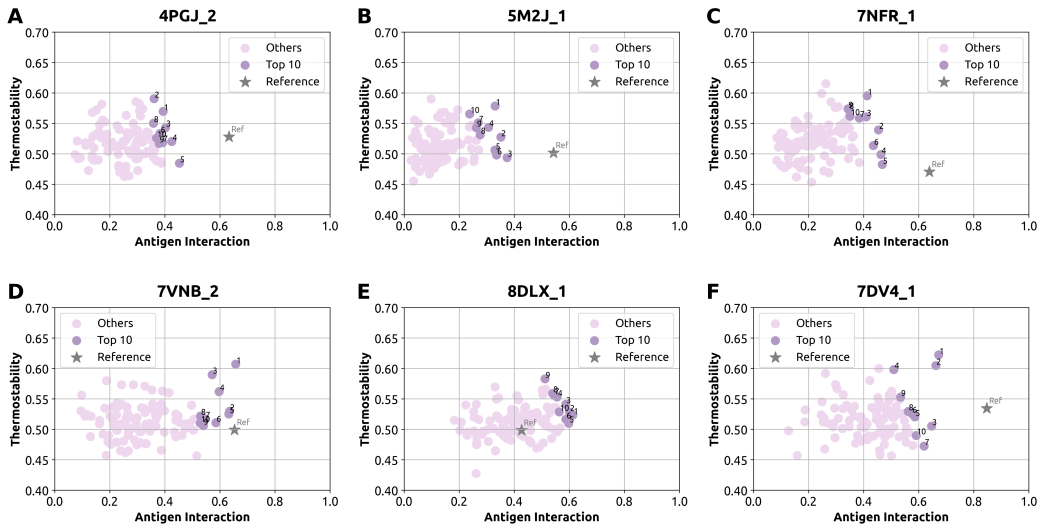


Figure A10: Scores of MCTS-generated nanobodies with antigens (topK=100). The antigens shown here are the same as in A7. The ones in A-E are with a experimental nanobodies that exhibit moderate interaction scores (0.4-0.65).